Experimental Charge Density of α-Glycine at 23 K

Riccardo Destro,*,† Pietro Roversi,†,‡ Mario Barzaghi,† and Richard E. Marsh*,§

Contribution from the Beckman Institute, California Institute of Technology, Pasadena, California 91125, and Department of Physical Chemistry and CSRSRC Center of the CNR, University of Milan, 20133 Milano, Italy

Received: September 30, 1999

The electrostatic properties of crystals of α-glycine have been obtained from extensive X-ray diffraction data collected at approximately 23 K and carefully processed, including corrections for scan truncation losses, anisotropic extinction, and multiple reflection. From a multipole parameterization of the X-ray intensities we have obtained an unusually precise—and we are confident, accurate—model of the total electron distribution in the crystal including the topological features, atom and group charges, the dipole moment for the glycine zwitterion, electrostatic potentials, electric field gradients at the nucleii of the three hydrogen atoms of the ammonium group, and intermolecular electrostatic energies within the crystal. We have also calculated the total interaction energies involving the six distinct types of intermolecular pairings and examined these energies in terms of the molecular arrangement.

Introduction

The experimental determination, by X-ray diffraction, of the total, static electron density in a crystal is a field of increasing interest. With this technique, many important properties can be derived, including reliable internuclear distances, atomic and group charges, bond critical points, dipole and quadrupole moments, electrostatic potentials, electric field gradients, and intermolecular electrostatic energies within the crystal. In parameterizing the electron density distribution, measured X-ray diffraction intensities are usually interpreted in terms of three types of functions: (i) spherical functions, describing the distribution of inner shell electrons plus the spherically-symmetric component of the valence electron distribution; the centers of these functions are presumed to define the positions of the atomic nucleii; (ii) deformation functions, usually multipoles, representing the aspherical distribution of the valence electrons; (iii) anisotropic displacement parameters (ADPs), describing effects such as thermal motion, molecular librations, and other types of atomic displacements; these ADP's are usually interpreted as dynamic properties, although static displacements due to crystal imperfections may be included in them. Once the parameters describing these various functions have been adequately fit to the experimental intensities, those of type (i) and (ii) can be used to reconstruct the total, *static* electron distribution throughout the crystal, $\rho(r)$.

A crucial aspect of this treatment involves the ability to clearly separate the ADPs (iii) from the static parameters (i) and (ii), and in particular from the deformation functions (ii). For this purpose, high-angle intensity data (minimum interplanar spacing, 0.5 Å or less) are necessary; for organic crystals, such data are usually available only at reduced temperatures. While recent experiments[1] have demonstrated that adequate data can be obtained at about 100 K, there is an added advantage of going to much lower temperatures: the ADPs, and hence, their effects on the static functions, are reduced to a minimum. Another requirement for an accurate description of the deformation functions (which contain essentially all the available information concerning the distribution of valence electrons) is that the low-angle intensity measurements be highly reliable.

Previous diffraction experiments on glycine crystals (α form) include early photographic studies using Cu Kα and Mo Kα X-radiation,[2,3] two neutron-diffraction studies,[4] and combined neutron and X-ray studies at room temperature[5] and at 120 K.[6] While studies of molecular geometry and thermal motion were the main objects of these investigations, a partial comparison between calculated (by ab initio methods) and experimental features of the electron density was reported,[5] based on "X−N" deformation maps of the differences between the electron densities as measured by X-ray diffraction and the nuclear densities as measured by neutron diffraction, both at room temperature. Subsequently, the 120 K data[6] were analysed in terms of deformation maps. Quite recently, these same data were used as a test case for the application of a two-channel maximum-entropy-method (MEM) to the electron deformation density.[7] As far as we are aware, only a rather limited account has been published[8] on the topological features of $\rho(r)$ based on these 120 K data.

In this paper we present the results of an extensive and, in our opinion, a very careful experimental study of the electron density distribution in α-glycine. In view of the rather special care that we have taken in the collection and interpretation of the experimental data, we describe our efforts in a bit more detail than usual.

Experimental Section

Data Collection and Processing. A suitable fragment of a prismatic crystal, grown by evaporation of an aqueous solution, was shaped into an almost perfect sphere of radius 0.26 mm by carefully rounding off all edges with damp paper under a microscope. After the quality of the crystal was checked by diffraction photographs, it was mounted on a four-circle diffractometer equipped with a Samson cryostat,[9] where the crystal is enclosed in an evacuated, nearly isothermal cavity. The temperature was maintained at approximately 22.6 K (with

† University of Milan.
‡ Present address: Structural Studies Division, MRC-LMB Cambridge, England, U.K.
§ California Institute of Technology.

10.1021/jp993505o CCC: $19.00 © 2000 American Chemical Society
Published on Web 01/13/2000

TABLE 1: Unit Cell Dimensions at Several Temperatures: Space Group, $P2_1/n$

temperature (K)	a (Å)	b (Å)	c (Å)	β (degrees)	volume (Å^3)
23	5.087(2)	11.773(5)	5.460(2)	111.99(3)	303.2(2)
70	5.088(2)	11.787(5)	5.460(2)	111.98(3)	303.6(2)
120	5.090(2)	11.816(4)	5.459(2)	111.93(3)	304.6(2)
170	5.093(2)	11.851(4)	5.460(2)	111.88(2)	305.8(2)
228	5.098(2)	11.897(4)	5.461(2)	111.81(2)	307.5(2)
291	5.105(1)	11.964(3)	5.462(2)	111.73(2)	309.9(1)

a maximum fluctuation of 1.2 K) during the 3-week period of data collection. Unit-cell dimensions at this temperature were obtained from the setting angles of 7 Friedel-related pairs of medium-angle ($42° < 2\theta_{Mo} < 46°$) reflections, measured before, during, and after the intensity measurements. Cell dimensions were also measured several times at room temperature, before and after cooling the crystal. Subsequently we measured the cell dimensions at several intermediate temperatures; the values are summarized in Table 1. There is no indication of a phase transition in the range 23−291 K.

Intensity data for the hemisphere $h \geq 0$ were collected at 23 K using graphite-monochromatized Mo Kα radiation ($\lambda = 0.71073$ Å) out to $2\theta = 109°$ ($\sin\theta/\lambda = 1.15$Å^{-1}). The two quadrants $k \geq 0$ and $k \leq 0$ were collected in separate steps, with warming of the crystal to about 140 K in between (to assure that hysteresis was not a problem). Low-angle data ($2\theta \leq 45°$) were then remeasured at a lower current setting to minimize possible problems associated with nonlinearity of the counting system, and 1100 background measurements were made at points distant from any reciprocal-lattice point. Finally, 18 reflections which, during the course of the refinement, appeared to have been affected by multiple reflection (Renninger effect) were later recollected at different crystal orientations. The total number of intensity measurements was 10891, each recorded with $\omega/2\theta$ scans at a scan rate of 3°/min in 2θ and a 2θ scan range of $(2.5 + \Delta)°$, where Δ is the $K\alpha_1,\alpha_2$ separation. Backgrounds were measured before and after each scan.

All intensity measurements were corrected for scan-truncation losses according to our empirical method[10] based on profile analyses of about 400 strong reflections measured at enlarged scan ranges. The background distribution as a function of 2θ (a crucial quantity in the truncation−correction procedure) was obtained separately from the 1100 background measurements and from the background counts measured for the very weak reflections; the two distributions agreed within statistical uncertainty. The largest scan-truncation losses, for reflections with $2\theta > 100°$, amounted to about 12% of the measured intensities. (It is our belief that these truncation errors are responsible, in many instances, for the systematic differences between displacement parameters often obtained in parallel neutron and X-ray diffraction studies.) Absorption was ignored ($\mu r = 0.02$).

Experimental variances σ_I^2 were based on counting statistics plus an additional term $(0.015S)^2$, where S is the scan count; this term was suggested by the fluctuations of the intensities of three standard reflections. Weighted averaging of multiple observations yielded 3822 independent values of F_{obs}^2, of which 33 were negative. The value of R(merge) was 0.015 for the 3776 nonnegative reflections measured more than once.

As shown by Denne in his extensive study[11] of six crystals of α-glycine of various shapes and sizes, the diffraction intensities of the stronger reflections are seriously affected by extinction. In our case, we accounted for extinction by adopting an anisotropic model for a Type I crystal[12] with a Lorentzian distribution of mosaicity as described by Thornley and Nelmes.[13] The six components of the G tensor were obtained from a least−squares fit to the ψ-scan measurements of 140 low-angle reflections, carried out at an intermediate stage of the multipole refinement. The principal values of this G tensor correspond to mosaic spreads ranging from 0.6 to 3.4 s of arc.

Refinement. Preliminary full-matrix least-squares refinement was based on a conventional spherical-atom model starting with the room-temperature coordinates of Marsh;[3] after convergence was reached, the multipole formalism of Stewart[14] was introduced to take account of asphericities in the electron distributions. Several different models were tested; the most satisfactory one included multipoles up to the hexadecapole level for the C, N and O atoms and to the quadrupole level for the H atoms. Core and valence electron monopole functions were from the Hartree−Fock expansions of Clementi,[15] with the population parameters of the core electrons constrained to be equal for C, N, and O. Radial terms for the higher multipoles were of the form $r^n\exp(-\alpha r)$, with $n = 2$, 2, 3, and 4 for dipoles, quadrupoles, octupoles, and hexadecapoles, respectively. Values of α, as obtained from some preliminary least-squares refinements, were 2.82 bohr^{-1} for C, 3.11 for N, and 5.15 for O. Initial scattering factors for H were those of the H_2 molecule,[16] and their coordinates and isotropic U's were allowed to shift; subsequently, these final coordinates were fixed and generalized monopole and dipole functions were introduced ($n = 0$ for monopole and 1 for dipole, $\alpha = 2.48$ bohr^{-1}). Finally, anisotropic U^{ij}'s (ADP's) were introduced for the H atoms, based on spectroscopic information and the molecular rigid-body librations derived from the refined ADP's of the C, N, and O atoms, as was done in a previous study of citrinin.[17] Quadrupoles could then be introduced for the H atoms, with $n = 2$ and $\alpha = 2.48$ bohr^{-1}. The total number of parameters was 216. The overall scale factor was not among the parameters; it was adjusted at the end of each cycle to be equal to the sum of all monopoles divided by $F(000) = 160e^-$.

All refinements were carried out with the VALRAY set of programs,[18] based on the 3789 reflections with $F_{obs}^2 > 0$. In assigning weights, the experimental variances σ_I^2, propagated over all contributing measurements of a reflection, were augmented by a term $(0.014\hat{I})$, in order to reduce the influence of reflections that were measured many times. Convergence was assumed when the sum of weighted residuals, ϵ, changed by less than 1.3 parts in 10^6. All second derivatives of ϵ were included in the last cycles in order to insure convergence to the correct minimum. The final value of the goodness-of-fit was 1.041. Other agreement indexes were $R_F = 0.0129$ and $R_{F^2} = 0.0172$; for the 697 reflections with $\sin\theta/\lambda \leq 0.65$ Å^{-1}, which are so crucial to the mapping of the valence-electron distribution, the corresponding numbers are 0.0097 and 0.0205.

Results and Discussion

The low values of the agreement indicators give us good confidence in our results. Another key point in assessing the reliability of charge density studies involves the problem of correlations between various parameters; as noted earlier, this is the reason why high-angle and low-temperature data are a necessity. In the present case we are pleased that only 27 correlation coefficients exceed 0.5 in absolute magnitude and only 6 exceed 0.7; the largest (0.74) relates a quadrupole component of an oxygen atom with the corresponding ADP and the next largest, 0.72, relates a dipole (also of an O atom) with the corresponding coordinate. As a result, estimated standard deviations (esd's) are small (and, we believe, reliable); the esd's

TABLE 2: Atom Coordinates, U_{eq} Values, and Charges

atom	*x*	*y*	*z*	U^a_{eq}	charge
C(1)	0.069 33(2)	0.125 16(1)	0.065 79(2)	0.003 98(1)	−0.10(2)
C(2)	0.057 97(2)	0.145 85(1)	−0.214 06(2)	0.004 93(1)	−0.20(2)
N	0.294 96(2)	0.088 38(1)	−0.259 56(2)	0.005 17(1)	−0.27(2)
O(1)	0.302 08(2)	0.093 79(1)	0.236 42(2)	0.005 61(1)	−0.41(1)
O(2)	−0.155 23(2)	0.142 38(1)	0.106 55(2)	0.005 94(1)	−0.46(1)
H(1)	0.277 6(11)	0.100 3(4)	−0.452 9(12)	0.019	+0.33(1)
H(2)	0.488 4(12)	0.117 0(4)	−0.133 8(11)	0.015	+0.34(1)
H(3)	0.289 5(8)	0.002 9(5)	−0.226 6(8)	0.016	+0.31(1)
H(4)	0.074 9(8)	0.236 0(4)	−0.241 6(8)	0.020	+0.22(1)
H(5)	−0.141 7(11)	0.114 9(4)	−0.359 0(10)	0.018	+0.24(1)

[a] The ADPs for the H atoms are calculated values (see text).

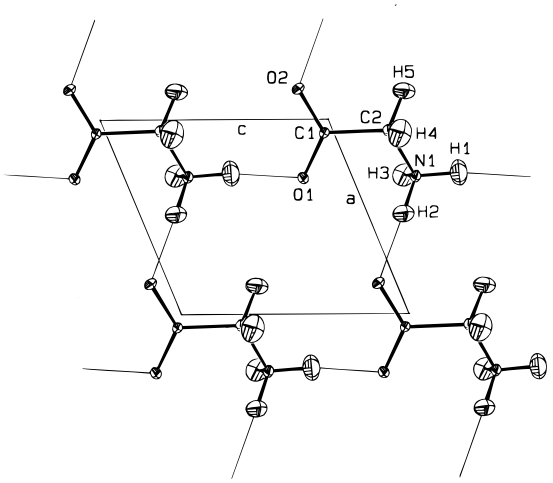

Figure 1. A layer of glycine molecules viewed down the *b* axis, with the atomic numbering scheme. Ellipsoids at 75% probability level. Thin lines connecting the ellipsoids of H and O atoms represent hydrogen bonding.

of the coordinates and ADPs of the C, N, and O atoms are about 20% as large as those obtained at 120 K.[6]

Molecular Geometry. Glycine crystallizes as a zwitterion, $NH_3^+CH_2COO^-$, with four molecules in a monoclinic cell, space group $P2_1/n$. Atom coordinates are given in Table 2.

Two strong hydrogen bonds form layers of molecules perpendicular to the *b* axis (Figure 1); adjacent layers are held together by a third, somewhat weaker hydrogen bond and by an additional N−H···O interaction which is usually categorized as a short van der Waals contact. Bond lengths and angles involving C, N, and O are in Table 3, where we include values found in earlier studies at higher temperatures.[3,4,6] (We emphasize that these bond lengths and angles refer to *zwitterionic* glycine, in a crystal with extensive hydrogen bonding, and that comparison with theoretical values for an isolated molecule is unproductive.) Comparisons among the three temperatures show the usual trend: covalent bonds appear to lengthen slightly with decreasing temperature, as the effects of molecular libration decrease, while intermolecular distances contract along with the cell dimensions. (The strongest hydrogen bond, N···O1, shortens only slightly with temperature; the weak out-of-plane bond N···O2 becomes appreciably shorter.)

Coordinates of the hydrogen atoms are difficult to discuss, since the positions of the nucleii cannot be measured. Our coordinates agree with those obtained by Kvick in an early neutron investigation at 15 K[19] within, on average, 2.3 esd's. Our N−H and C−H distances are shorter, by 0.01−0.02 Å, than those found by Kvick.

Molecular Motion. The principal values of the **U** tensors (mean-square displacements) for the C, N, and O atoms are, on average, 43% as large at 23 K as they are at 120 K[6] which are, in turn, about half as large as those at room temperature;[5] the esd's of these parameters are about 20% as large as those at 120 K and 4% as large as those at room temperature. A rigid-body TLS analysis[20] resulted in calculated values of the U^{ij}'s differing from the observed ones by, on average, about 4 esd's. It is likely that much of this discrepancy is due to various bond-bending displacements, which we have not attempted to analyze for this asymmetric, strongly hydrogen-bonded system. We also note that, if we compare the mean-square displacements of pairs of bonded atoms in the directions of the bonds between them (which should be identical for a rigid bond), we find an average difference of only 0.00024 Å^2, well below the value of 0.001 Å^2, which Hirshfeld has suggested as indicating adequate agreement with a rigid-bond postulate.[21] The major components of the molecular motions appear translational in character, with root mean-square (rms) amplitudes of about 0.06 Å in all directions, approximately the same as those found in a similar study of *l*-alanine.[22] The eigenvalues of the librational tensor **L** are 8.9, 3.5, and 1.7 deg^2, somewhat larger than in the bulkier *l*-alanine, 4.9, 2.6, and 2.3 deg^2. Implied corrections to bond lengths should amount to less than 0.002 Å for both amino acids.

TABLE 3: Bond Lengths (angstroms)[h], Bond Angles (degrees), and Short Intermolecular N···O Distances (angstroms)

bond	23 K[a]	120 K[b]	*RT*[c]
C(1)−O(1)	1.2570	1.2562	1.252
C(1)−O(2)	1.2593	1.2580	1.255
C(1)−C(2)	1.5269	1.5238	1.523
C(2)−N	1.4823	1.4796	1.474
angle	**23 K[a]**	**120 K[b]**	***RT*[c]**
C(2)−C(1)−O(1)	117.44	117.36	117.4
C(2)−C(1)-O(2)	117.02	117.17	117.1
O(1)−C(1)−O(2)	125.54	125.46	125.5
C(1)−C(2)−N	111.50	111.69	111.8
distance	**23 K[a]**	**120 K[b]**	***RT*[c]**
N···O(1)[d]	2.7664	2.7667	2.769
N···O(2)[e]	2.8347	2.8327	2.853
N···O(2)[f]	3.0048	3.0200	3.076
N···O(1)[g]	2.9366	2.9361	2.953

[a] This investigation; esd's ≈ 0.0005 Å and 0.02°. [b] Reference 6; esd's ≈ 0.0007 Å and 0.02°. [c] Weighted averages of refs 3, 4a, and 4b; esd's ≈ 0.001 Å and 0.03°. [d] At (x, y, z − 1.0). [e] At (x + 1.0, y, z). [f] At (−x, −y, −z). [g] At (1.0 −x, −y, −z). [h] For the 23 and 120 K studies, the esd's reflect primarily the uncertainties in the cell dimensions rather than in the atom coordinates.

Group Charges and Dipole Moment. The charges on the individual atoms, taken as the sum of the monopole populations less the atomic number, are included in Table 2; from them we evaluate the charges on the three atom groupings in the glycine zwitterion: CO_2, $-0.97(3)e^-$; NH_3, $+0.72(3)e^-$; and CH_2, $+0.26(3)e^-$. These values are approximately twice those derived[23] from deformation density distributions obtained from diffraction data at 120 K,[6] and they are closer to those obtained from various theoretical treatments.[24] The dipole moment, evaluated from the monopole and dipole populations of the various atoms, is 14.9(3) D; not surprisingly, its direction is approximately parallel to the principal axis of the molecule (and to the *c* axis of the crystal). Other experimental values,[25] all of which refer to aqueous solutions, range from 11.6 to 15.7 D with uncertainties (when reported) of 0.3−0.7 D. We are not aware of any critical discussion or comparison of these values, which come from different experimental techniques including the Kerr effect, isopiestic vapor pressure, and dielectric measurements. A hasty survey seems to indicate that the differences among

the reported values originate in different approximations and models applied to the measured quantities rather than in different reliabilities of the measurements. Published theoretical estimates[24b,26] range from 10.8 to 15.6 D, all referring to an isolated, zwitterionic species. The smallest values[26a] are based on optimized geometries for the isolated molecule and are not comparable with those found in crystals; the largest estimate, 15.64 D, comes from a charge scheme tailored for molecular mechanics[26b] and based not on bond lengths and angles but only on group charges (the predicted value for alanine is practically the same as that for glycine). An intermediate value, 13.85 D, was obtained from ab initio calculations[26c] with a split-valence 6-31G basis set and bond lengths and angles taken from the standard values given by Pople and Gordon;[27] when based on the room-temperature neutron diffraction geometry,[4a] ab initio calculations with four different basis sets[24b] gave values in the range 13.0−13.7 D, and the semiempirical CNDO/2 method led to a value of 13.2 D. The somewhat larger value that we find in the crystal presumably reflects the enhancement in charge due to intermolecular interactions, as observed in many other instances.[28]

Topological Properties of $\rho(r)$. The experimental electron distribution in the glycine crystal can be analyzed in terms of its topological features in the same way that theoretical charge distributions are analyzed in Bader's theory of atoms in molecules.[8b] The quantities used to describe ρ(r) are the number and kind of critical points (where $\nabla\rho = 0$); the values of ρ and of its principal curvatures λ_1, λ_2, and λ_3 (eigenvalues of the Hessian function of ρ) at these critical points; and the value of the Laplacian $\nabla^2\rho = \lambda_1 + \lambda_2 + \lambda_3$. The main focus is on *bond* critical points, bcp's, at which one curvature (λ_3, along the bond path) is positive and the other two are negative; the ratio of the latter two curvatures defines the bond ellipticity ϵ [$(\lambda_1/\lambda_2) - 1$, with $\lambda_1 < \lambda_2$]. For covalent bonds, the bond path is expected to be effectively coincident with the line between the two nucleii, as found in an extensive topological analysis of the experimental density in citrinin crystals.[17]

Plots of $\rho(r)$ and its Laplacian in the plane of the carboxylate group in glycine are shown in Figure 2; properties of the critical points associated with the covalent and hydrogen bonds and with some short intermolecular contacts are in Table 4. While the *precisions* in the positions of the bcp's are good, with esd's (as propagated from the results of our final least-squares refinements) of about 0.002 Å, our experience indicates that the positions are model-dependent, being particularly sensitive to the values of α adopted in the multipole descriptions. For example, in glycine we find the bcp's of the C−O bonds to be about 35% of the distance along the lines from C to O, while in *l*-alanine,[22] where we chose a larger value of α for the C atoms and a smaller one for O, they were at about 42% of the distance. The positions of the critical points in the C−C and C−N bonds are approximately the same in glycine and *l*-alanine, lying close to the center of C−C but shifted toward the less-charged atom, C2, in the N−C bond. In the three N−H bonds the critical points are about three-fourths of the distance along the bonds; for the two C−H bonds, involving H atoms with smaller charges, they are at about two-thirds of the distance. The values of ρ at the critical points of the C−O bonds lie well within the range 2.64−2.87 eÅ^{-3} compiled for carboxylate groups of other amino acids,[1c] and are close to the value of 2.70 eÅ^{-3} predicted from an empirical correlation noted by Roversi et al.;[17] the marginally significant difference between the ρ_c values of these two bonds follows the correlation. (The C−O1 bond in *l*-alanine was omitted from the compilation;[1c] it is quite short, at 1.248 Å, and ρ is large, at 3.02 eÅ^{-3}.) Critical-point parameters of the C−C and C−N bonds are also within the range in other amino acids[1c] with the exception of a slightly higher value for the Laplacian for the C−C bond, perhaps reflecting the presence of the second hydrogen atom in glycine. The eccentricities of all the covalent bonds are small. We note that the eigenvectors associated with the λ_2 values—the smaller of the negative curvatures, in an absolute sense—of the C−C and the two C−O bond critical points are all approximately perpendicular to the plane of the carboxylate group, suggesting some conjugation in this grouping. Values of the Laplacian at the critical points of the two C−O bonds follow the expected trend, the slightly shorter C−O1 bond having the slightly more negative Laplacian. In *l*-alanine the differences are more pronounced, the short C−O1 bond of 1.248 Å showing a Laplacian of −39.0 eÅ^{-5} and the longer C−O2 of 1.267 Å, −29.6 eÅ^{-5}. Surprisingly, our values for the Laplacians

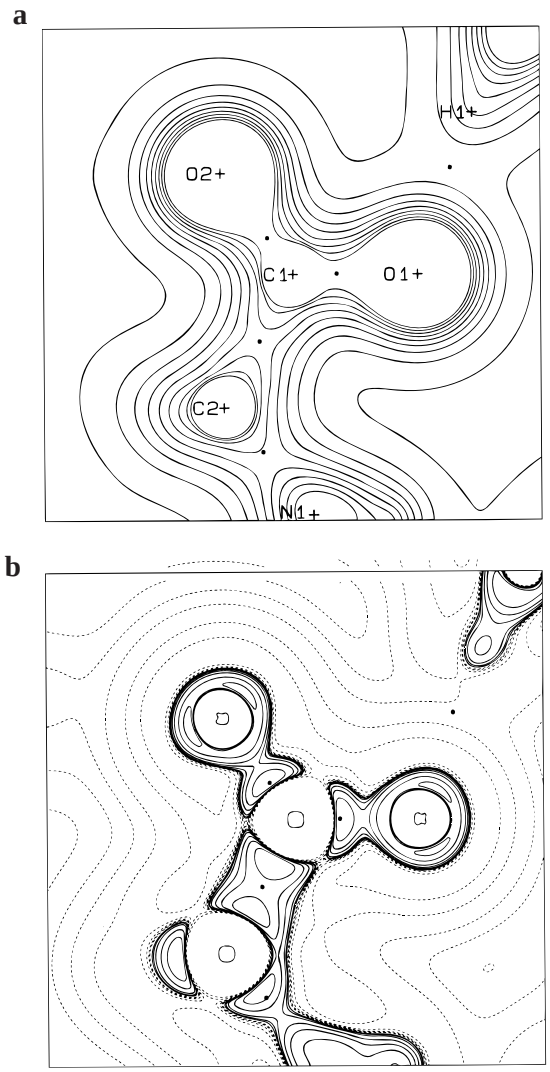

Figure 2. Maps (5 × 5 Å) of (a) the experimental electron density ρ and of (b) its negative Laplacian $-\nabla^2\rho$ in the plane of the carboxylate group of glycine. Atoms C2 and N1 are displaced from the plane, in opposite directions, by 0.02 and 0.42 Å, respectively. Atom H1 belongs to the molecule at x, y, $1 + z$, and is 0.27 Å out of plane. Contour levels for ρ are at intervals of 0.3 e Å^{-3}, from 0.1 (outermost contour) up to 2.50 e Å^{-3}. The Laplacian is plotted, at variable intervals, in units e Å^{-5}. Short dashed lines describe the positive region (charge depletion) of $\nabla^2\rho$, solid lines the negative region (charge concentration). The five asterisks in each map locate the bond critical points of ρ; two of them, out of plane (for C2−N and O1···H1 interactions), have been projected onto the plane.

TABLE 4: Properties of Bond Critical Points in α-Glycine[a]

bond (a−b)	d^b	$R_a{}^c$	ρ	$\nabla^2\rho$	λ_1	λ_2	λ_3	ϵ^d
intramolecular bonds								
C1−O1	1.257	0.443	2.77(2)	−32.8(9)	−26.93	−25.09	19.18	0.07
C1−O2	1.259	0.447	2.67(2)	−30.5(9)	−25.51	−22.60	17.66	0.13
C1−C2	1.527	0.772	1.78(1)	−15.6(4)	−13.55	−12.17	10.10	0.11
C2−N	1.482	0.632	1.69(1)	−11.9(5)	−12.27	−11.77	12.18	0.04
N−H1	1.035	0.779	2.20(2)	−35.4(13)	−30.83	−30.41	25.82	0.01
N−H2	1.023	0.770	2.21(2)	−36.2(13)	−32.05	−29.69	25.61	0.08
N−H3	1.024	0.762	2.24(2)	−33.0(11)	−30.09	−29.75	26.86	0.01
C2−H4	1.080	0.719	1.99(1)	−22.7(6)	−19.78	−19.37	16.50	0.02
C2−H5	1.090	0.716	1.91(2)	−21.2(7)	−18.68	−17.98	15.43	0.04
hydrogen bonds								
O1···H1′	1.748	1.130	0.286(9)	2.47(18)	− 1.91	−1.83	6.21	0.04
O2···H2′	1.821	1.177	0.215(9)	2.25(17)	−1.49	−1.18	4.92	0.26
O2···H3″	2.039	1.283	0.125(6)	1.59(9)	−0.66	−0.60	2.85	0.10
short intermolecular contacts								
O1···H3″	2.387	1.398	0.057(3)	1.18(2)	−0.24	−0.21	1.63	0.09
O2···H4′	2.340	1.389	0.067(4)	1.07(3)	−0.27	−0.23	1.57	0.17
O1···H4″	2.415	1.432	0.059(4)	0.96(3)	−0.24	−0.18	1.37	0.33

[a] Distances (d and R_a) in angstroms; ρ and $\nabla^2\rho$ in units of e Å^{-3} and e Å^{-5}, respectively. Esd's for λ's are, on average, about half those of $\nabla^2\rho$. [b] Interatomic distance. [c] Distance from the first atom of the pair to the critical point; esd's of about 0.002 Å. [d] Ellipticity, defined as $(\lambda_1/\lambda_2) - 1$.

associated with the C−O bonds are seriously at odds with those obtained[8] from a Hirshfeld treatment[29] of 120 K data, which were *positive* for both bonds. The Laplacians for the C−C and C−N bonds in that investigation do not differ greatly from ours.

We note that all three N−H bonds in glycine show, within experimental error, the same values of ρ and $\nabla^2\rho$ at their critical points. Perhaps remarkably, these values differ by less than 3 esd's from those found in the ammonium grouping of methylammonium hydrogen succinate,[14b] where the H atoms were located from neutron diffraction data; similar agreement is also observed for the C−N and C−H bonds in the two compounds. These positive comparisons increase our confidence in our treatment of the H atoms and in our overall model of the electronic properties of glycine.

The critical points of the noncovalent interactions, H···O (Table 4), all share the same features of low values for ρ, decreasing as the interatomic separation increases, and of positive values of $\nabla^2\rho$, indicative of closed shell interactions or ionic-type bonding; as usual in these cases, the Laplacian is dominated by the positive curvature along the internuclear line. Interestingly, for all six such interactions in glycine the behaviour of $\nabla^2\rho$ as a function of ρ is very close to that recently predicted by Spackman[30] from a simple model of noninteracting overlapping spherical atomic electron densities. The critical points of five of these interactions lie within 0.06 Å of the straight line between O and H; that associated with O1···H3 is displaced by 0.24 Å. We see no topological feature, of those reported in Table 4, that would distinguish a conventional hydrogen bond from a short van der Waals contact except, perhaps, the distance of the critical point from the O atom, 63−65% of the O···H distance for the three true hydrogen bonds in glycine and 59% for the other three interactions. On the other hand, if the criteria devised by Koch and Popelier[31] for quantum−topological analysis are adopted for our experimental charge density distribution, the two C−H···O interactions in Table 4 would be classified as hydrogen bonds. Further aspects of the intermolecular interactions between glycine molecules will be discussed in a following section.

An overall view of the deformations to the electron density caused by the formation of bonds or other interatomic interactions can be seen in Figure 2a and also in the Laplacian mapping, Figure 2b, which shows the pattern of changes in charge distribution. The lone-pair charge concentrations on the oxygen atoms are clearly shown in Figure 2b; these features are similar to those we have previously seen on other charge density studies based on high-quality X-ray data measured at 19−23 K.[17,22,32]

Electrostatic Potential. The electrostatic potential at any point **r** can be evaluated from the expression

$$\Phi(\mathbf{r}) = \int \rho(\mathbf{r}')|\vec{r} - \vec{r}'|^{-1} d\mathbf{r}'$$

where the vectors $\vec{r}$ and $\vec{r}'$ have a common, arbitrary origin. For a crystal, two types of electrostatic potentials can be derived: (1) the potential associated with a single molecule removed from the crystal, for which the integral is over the electron (and nuclear) density of a single molecule and (2) the total potential for the crystal, where the integral extends over the entire, repeating structure (to values of $\mathbf{r}'$ where the denominator becomes overwhelming). The mathematical formalisms implemented in VALRAY[18] to derive $\Phi(\mathbf{r})$ are due to Stewart, who first outlined the procedure[33] and then described it in detail in an analysis of γ-aminobutyric acid.[34] The potential for an isolated molecule is conveniently derived from $\rho(\mathbf{r})$ as obtained from the multipole functions. For the total crystal potential it is more convenient to treat the spherical functions as above but to describe the deformation components by means of a Fourier summation with coefficients $\Delta F = F_{multipole} - F_{IAM}$: the differences between structure factors calculated for the total multipole model and those calculated for a spherical, independent-atom model; an "inner potential" term, Φ_{inner}, is subtracted to provide contrast in the otherwise all-positive map. Sections through these two potential mappings are shown in Figure 3.

Figure 3a clearly shows the separation between the strongly electronegative region of the molecule CO_2^- and the strongly positive $CH_2NH_3^+$. The minimum in the map, at −563(35) kJ mol$^{-1}e^{-1}$, is 1.086 Å from O2, in a direction that forms an angle of 111° with the C−O bond, almost exactly at the same place as the minimum potential (−500(42) kJ mol$^{-1}e^{-1}$) in *l*-alanine.[22] (At first glance, the two maps appear virtually identical.) The hydrogen-bonding pattern in the two compounds is noticeably different, so the feature of deeper minima for O2 over O1 appears not to be related to hydrogen bonding but rather to the larger negative charge on O2. Figure 3b indicates that, in the crystal, the glycine zwitterion is completely surrounded by regions of negative potential, all relatively flat except for a small region along the H1···O1 hydrogen bond, which lies almost exactly in the plane of the map.

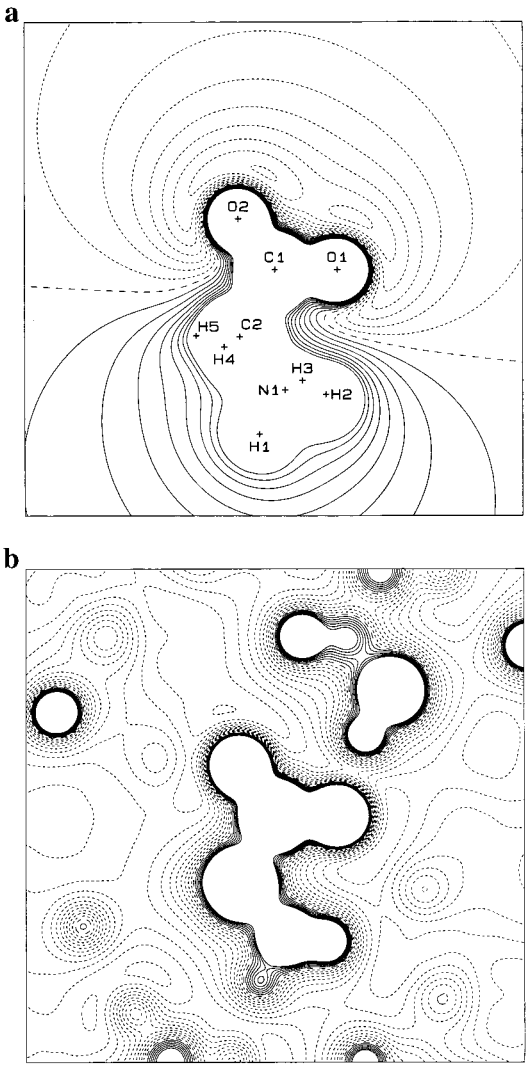

Figure 3. Electrostatic potential of glycine, as obtained from the diffraction experiment at 23 K. Contour maps (10 × 10 Å) in the COO plane are shown for (a) the potential of a molecule extracted from the crystal, and for (b) the total potential in the crystal. Contour intervals are 0.05 $|e|$ Å^{-1} (1 $|e|$ Å^{-1} = 1389 kJ mol^{-1} $|e|^{-1}$); solid lines positive, short dashed lines negative, large dashed lines zero contour.

Energies of Molecular Interactions. Each molecule of glycine in the crystal is in direct contact with ten other molecules, related by various symmetry operations; there are six distinct *types* of interactions between pairs of molecules. (Four types of pairings, those involving translational symmetry operations, are duplicated, since the parent molecule must have equivalent interactions in both directions of translation.) We have evaluated the energies involved in each of these six types of pairings, using a computer program[35] based on the application of a model devised by Spackman et al.[36] In this model, the total interaction can be expressed as the sum of five terms

$$E_{\mathrm{tot}} = E_{\mathrm{es}} + E_{\mathrm{pen}} + E_{\mathrm{rep}} + E_{\mathrm{dis}} + E_{\mathrm{HB}}$$

representing electrostatic, penetration, repulsion, dispersion, and hydrogen-bonding energies. Details of the assumptions on which this model is based are given by Spackman et al.;[36] we only note that a hydrogen bond is described by omitting the atom−atom potential terms between the proton and its acceptor—a procedure which "appears to be equivalent to the addition of an extra attractive term in our energy expression, along with retention of all exp(-6) atom−atom potential terms".[37]

We have evaluated the energies for the six different types of molecular pairings in glycine; they are given in Table 5, arranged in the order of increasing distance between the centers of mass of the two molecules. Five of the six pairings are shown in Figure 4, where the molecules are labelled to correspond to the pairs in Table 5; the unlabelled molecule is one of each pair. (These are the same pairings as those represented by O−H interactions in Table 4.) We see that the electrostatic energy, E_{es}, is the major component of all but one (pair D) of the interactions. This term, which is a classical interaction between the charge distribution on one molecule and the electrostatic potential Φ of the other, can be easily evaluated in this procedure, as can its esd, which is seldom possible for energies.

Pair A shows the largest total attractive energy, 200 kJ mol^{-1}; while this pairing involves the weakest of the three true hydrogen bonds, the bond occurs twice because of a center of inversion (pair C also includes a center of inversion). It seems surprising that pair D, which includes a strong hydrogen bond, shows a slightly positive total energy. Because of the orientation of the two molecules, which are related by translation along the *a* direction (see Figure 1), there are several short interactions between atoms of similar charge, especially between the ammonium atoms H1 and H2 of the parent molecule and the methylene atom H5 of the molecule at D. For H1···H5, at 2.808 Å, the electrostatic term E_{es} is +47 kJ mol^{-1} and for H2···H5, at 2.605 Å, +50 kJ mol^{-1}. We note that pairing F, which also involves a lattice translation (along the *c* direction; see Figure 1), has energy values similar to those for pair D for all terms except the electrostatic term E_{es}, which is strongly attractive. Here, the translation is in the direction of the C1−C2 bond; the line connecting the negatively charged CO_2 group to the positive CH_2NH_3 group, and results in alternating charges along *c*. Similarly, pairing C shows numerous attractive electrostatic interactions, including O1···H2, at 2.838 Å and −71 kJ mol^{-1} and O1···H3, at 2.387 Å and −85 kJ mol^{-1}, which overcome some repulsive H···H interactions.

Pairs B and E involve *n*-glide operations, and intermolecular contacts tend to be relatively long. Pair E shows only one contact shorter than 3.0 Å, O2···H4 (2.340 Å), with an attractive component E_{es} of about −76 kJ mol^{-1} and a repulsive term E_{rep} of about 11 kJ mol^{-1}; all terms for this pairing are quite small. The shortest contact in pair B, O1···H4, is also attractive, at −56 kJ^{-1} but is offset by a number of repulsive H···H interactions which result in a total interaction between the two molecules that is highly repulsive.

We emphasize that these intermolecular energies cannot be interpreted in terms of crystal energies. For example, the energies B and E might suggest that the interaction between glide-related sheets is repulsive and that the crystal should not be stable. But the cohesive energy comes from long-range, electrostatic terms; if we include interactions involving the 112 neighboring molecules within 15 Å (center of mass) of the parent molecule, we calculate that the total energy between sheets is cohesive by some 25 kJ/mol. We are also aware of limitations in the model we have adopted, and that caution must be exercised in interpreting these results.[36] However, we feel confident that the general picture we have presented of the intermolecular energies and, particularly, of the electrostatic terms, which are dominant in this case, are reliable and informative.

Electric Field Gradients. Of the electrostatic properties that can be derived by X-ray diffraction data, electric field gradients (EFG's) at atomic nuclei may appear the most unreliable. As noted by Brown and Spackman,[38] EFGs are sensitive to charge

TABLE 5: Interaction Energies (kJ mol^{-1}) for Pairs of Glycine Molecules in the Crystal

pair[a]	D[b]	E_{tot}[c]	E_{es}[d]	E_{pen}	E_{rep}	E_{dis}	E_{HB}[e]	shortest intermolecular distance (Å)	
A	3.067	−200	−231(9)	3	125	−44	−53	O2···H3	2.039
B	4.290	104	94(5)	0	25	−15	0	O1···H4	2.415
C	4.703	−117	−149(6)	1	52	−21	0	H2···H3	2.340
D	5.087	14	2(8)	3	89	−21	−59	O2···H2	1.821
E	5.367	−29	−38(8)	0	19	−10	0	O2···H4	2.340
F	5.460	−118	−139(12)	3	120	−26	−76	O1···H1	1.748

[a] Symmetry operations relating the second molecule of a pair to the parent one (at x, y, z) are for A: $-x, -y, -z$. B: $-^1/_2+x, ^1/_2-y, -^1/_2+z$. C: $1-x, -y, -z$. D: $-1+x, y, z$. E: $^1/_2+x, ^1/_2-y, -^1/_2+z$. F: $x, y, -1+z$. [b] Distance (angstroms) between centers of mass of the two molecules in a pair. [c] Total interaction energy, equal to the sum of the five contributions reported on the same line. [d] Electrostatic energy, with esd in parentheses. [e] Hydrogen bond energy. There are two identical H bonds in pair A, each contributing to E_{HB} for −26.5 kJ mol^{-1}; only one H bond occurs in pairs D and F.

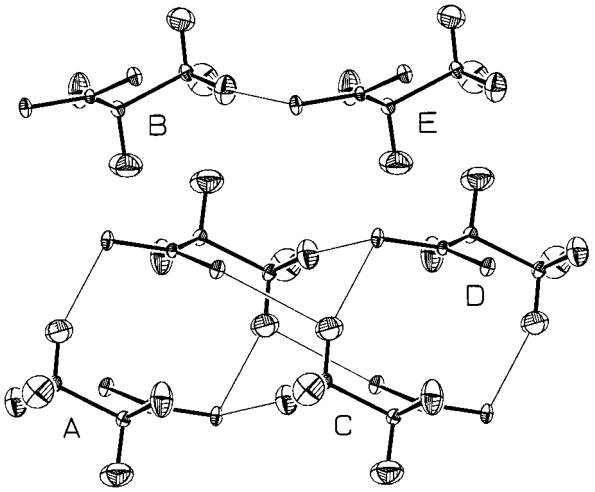

Figure 4. A view of the crystal structure of α-glycine perpendicular to the *a b* plane (*a* horizontal, *b* vertical), showing five of the six pairs of molecules for which the intermolecular interaction energy has been calculated. The unlabeled molecule is one of each pair; the label on each of the other five molecules identifies the pair. Symmetry operations relating the parent, unlabeled molecule to the other five are reported in Table 5.

TABLE 6: Quadrupole Coupling Constant QCC = e^2qQ/h and Asymmetry Parameter η for H and N Atoms of α-Glycine

	X-ray[a]		NQR[b]	
atom	QCC (kHz)	η	QCC (kHz)	η
H1	114	0.086	141.0	0.0355
H2	153	0.437	158.5	0.0473
H3	185	0.045	184.7	0.0217
N	663	0.056	1249	0.501

[a] Present work; QCC values calculated with quadrupole moments $Q_H = 0.28$ and $Q_N = 1.74$ fm^2. [b] From Tables 1 and 2 of ref 40.

density features involving core electrons which, to be accurately modeled, would require more extensive high-angle diffraction data than are currently available and a more flexible multipole model. The situation is not as severe for hydrogen atoms, which lack core electrons, but even for them additional multipoles would be needed.[39] As a result, while the orientations of the principal axes of the EFG tensors can be well determined from high-quality X-ray data, their magnitudes cannot.

We were pleasantly surprised, then, to find that the quadrupole coupling constants (derived from the largest principal component of the EFG tensor) for the three H atoms of the NH_3 group in glycine are in good agreement with the far more accurate values obtained from nuclear quadrupole resonance (NQR) measurements;[40] for two of the H atoms the asymmetry parameters η are also in good agreement (Table 6). Less satisfactory are the agreements for both the quadrupole coupling constant and the asymmetry parameter for the nitrogen atom.

Concluding Remarks

We have shown, through what we believe to be one of the most accurate charge-density studies yet carried out, the wealth of chemical information obtainable from a single-crystal X-ray diffraction experiment at very low temperature. In particular, by careful treatment of extensive high-quality intensity measurement and by assigning calculated ADPs to the hydrogen atoms we have been able to obtain electric field gradients at H nucleii which are in reasonable agreement with values obtained by NQR measurements. The topological analysis of the charge density has fully characterized the covalent and noncovalent bonds. Further development to be pursued in this area is the topological analysis of the Laplacian of the total electron distribution, a demanding task (especially in terms of data quality) essential for a better understanding of chemical reactivity.

Among the results we have presented, of particular relevance, in our opinion, is the experimental evaluation of electrostatic energies for the intermolecular interactions, with estimated uncertainties no larger than about 10 kJ mol^{-1}. The implications for studies of molecular modelling and recognition are evident.

Acknowledgment. Support of this work by the Italian MURST (ex 40%) is gratefully acknowledged by one of us (R.D.).

Supporting Information Available: Tables of atomic ADP's, components of the tensor of anisotropic extinction, and charge density parameters. This material is available free of charge via the Internet at http://pubs.acs.org.

References and Notes

(1) (a) Koritsánszky, T.; Flaig, R.; Zobel, D.; Krane, H.-G.; Morgenroth, W.; Luger, P. *Science* **1998**, 356−358. (b) Mallinson, P. R.; Woźiak, K.; Wilson, C. C.; McCormack, K. L.; Yufit, D. S. *J. Am. Chem. Soc.* **1999**, *121*, 4640−4646. (c) Coppens, P.; Abramov, Y.; Carducci, M.; Korjov, B.; Novozhilova, I.; Alhambra, C.; Pressprich, M. R. *J. Am. Chem. Soc.* **1999**, *121*, 2585−2593. (d) Spackman, M. A. *Ann. Rep. Prog. Chem., Sect. C: Phys. Chem.* **1997**, *94*, 177−207.

(2) Albrecht, G.; Corey, R. B. *J. Am. Chem. Soc.* **1939**, *61*, 1087−1102.

(3) Marsh, R. E. *Acta Crystallogr.* **1958**, *11*, 654−663.

(4) (a) Jönsson, P.-G.; Kvick, Å. *Acta Crystallogr., Sect. B* **1972**, *28*, 1827−1833; (b) Power, L. F.; Turner, K. E.; Moore, F. H. *Acta Crystallogr., Sect. B* **1976**, *32*, 11−16.

(5) Almlöf, J.; Kvick, Å.; Thomas, J. O. *J. Chem. Phys.* **1973**, *59*, 3901−3906.

(6) Legros, J.-P.; Kvick, Å. *Acta Crystallogr., Sect. B* **1980**, *36*, 3052−3059.

(7) Papoular, R. J.; Vekhter, Y.; Coppens, P. *Acta Crystallogr., Sect A* **1996**, *52*, 397−407.

(8) (a) Lau, C. D. H.; Bader, R. F. W.; Hermansson, K.; Berkovitch-Yellin, Z. *Chem. Scr. Abstr.* **1986**, *26*, 476; (b) Bader, R. F. W.; Laidig, K. F. *Trans. Am. Crystallogr. Assoc.* **1990**, *26*, 1−21.

(9) Samson, S.; Goldish, E.; Dick, C. J. *J. Appl. Crystallogr.* **1980**, *13*, 425−432.

(10) (a) Destro, R.; Marsh, R. E. *Acta Crystallogr., Sect A* **1987**, *43*, 711−718; (b) Destro, R. *Aust. J. Phys.* **1988**, *41*, 503−510; (c) Destro, R., Marsh, R. E. *Acta Crystallogr., Sect. A* **1993**, *49*, 183−190.

(11) Denne, W. A. *Acta Crystallogr., Sect A* **1972**, *28*, 192−201.

(12) Becker, P. J.; Coppens, P. *Acta Crystallogr., Sect A* **1975**, *31*, 417−425.

(13) Thornley, F. R.; Nelmes, R. J. *Acta Crystallogr., Sect A* **1974**, *30*, 748−757.

(14) (a) Stewart, R. F. *Acta Crystallogr., Sect. A* **1976**, *32*, 565−574; (b) Flensburg, C.; Larsen, S.; Stewart, R. F. *J. Phys. Chem.* **1995**, *99*, 10130−10141.

(15) Clementi, E. *IBM J. Res. Dev. Suppl.* **1965**, *9*.

(16) Stewart, R. F.; Bentley, J. J.; Goodman, B. *J. Chem. Phys.* **1975**, *63*, 3786−3793.

(17) Roversi, P.; Barzaghi, M.; Merati, F.; Destro, R. *Can. J. Chem.* **1996**, *74*, 1145−1161.

(18) Stewart, R. F.; Spackman, M. A. *VALRAY Users Manual;* Department of Chemistry, Carnegie−Mellon University: Pittsburgh, 1983.

(19) Kvick, Å. **1993**. Private communication.

(20) Schomaker, V.; Trueblood, K. N. *Acta Crystallogr., Sect. B* **1968**, *24*, 63−76.

(21) Hirshfeld, F. L. *Acta Crystallogr. A* **1976**, *32*, 239−244.

(22) (a) Destro, R.; Marsh, R. E.; Bianchi, R. *J. Phys. Chem.* **1988**, *92*, 966−973. (b) Destro, R.; Bianchi, R.; Morosi, G. *J. Phys. Chem.* **1989**, *93*, 4447−4457. (c) Destro, R.; Bianchi, R.; Gatti, C.; Merati, F. *Chem. Phys. Lett.* **1991**, *186*, 47−52.

(23) Berkovitch-Yellin, Z. *J. Am. Chem. Soc.* **1985**, *107*, 8239−8253.

(24) (a) Dixon, D. A.; Lipscomb, W. N. *J. Biol. Chem.* **1976**, *251*, 5992−6000. (b) Voogd, J.; Derissen, J. L.; van Duijneveldt, F. B. *J. Am. Chem. Soc.* **1981**, *103*, 7701−7706. (c) Boek, E. S.; Feil, D.; Briels, W. J.; Bennema, P. *J. Cryst. Growth* **1991**, *114*, 389−410.

(25) (a) Khanarian, G.; Moore, W. J. *Aust. J. Chem.* **1980**, *33*, 1727−1741. (b) Schrier, E. E.; Robinson, R. A. *J. Biol. Chem.* **1971**, *246*, 2870−2874. (c) Zhukov, V. V.; Stepin, L. D. *Biofizika* **1965**, *10*, 979−985. (d) Aaron, M. W.; Grant, E. H. *Trans. Faraday Soc.* **1963**, *59*, 85−89. (e) Hartmann, H.; Lertes, E.; Jaenicke, R. *Z. Naturforsch., Teil A* **1967**, *22*, 2118−2119.

(26) (a) Yu, D.; Armstrong, D. A.; Rauk, A. *Can. J. Chem.* **1992**, *70*, 1762−1772. (b) Abraham, R. J.; Hudson, B. *J. Comput. Chem.* **1985**, *6*, 173−181; (c) Wright, L. R.; Borkman, R. F. *J. Am. Chem. Soc.* **1980**, *102*, 6207−6210.

(27) Pople, J. A.; Gordon, M. *J. Am. Chem. Soc.* **1967**, *89*, 4253−4261.

(28) Spackman, M. A. *Chem. Rev.* **1992**, *92*, 1769−1797.

(29) (a) Hirshfeld, F. L. *Acta Crystallogr., Sect. B* **1971**, *27*, 769−781; (b) Harel, M.; Hirshfeld, F. L. *Acta Crystallogr., Sect B* **1975**, *31*, 162−172; (c) Hirshfeld, F. L. *Isr. J. Chem.* **1977**, *16*, 226−229.

(30) Spackman, M. A. *Chem. Phys. Lett.* **1999**, *301*, 425−429.

(31) Koch, U.; Popelier, P. L. A. *J. Phys. Chem.* **1995**, *99*, 9747−9754.

(32) Destro, R.; Merati, F. *Acta Crystallogr., Sect B* **1995**, *51*, 559−570.

(33) Stewart, R. F. *God. Jugosl. Cent. Kristalogr.* **1982**, *17*, 1−24.

(34) Stewart, R. F.; Craven, B. M. *Biophys. J.* **1993**, *65*, 998−1005.

(35) Spackman, M. A. Personal communication, 1990. Local version implemented by F. Merati and M. Barzaghi.

(36) Spackman, M. A.; Weber, H. P.; Craven, B. M. *J. Am. Chem. Soc.* **1988**, *110*, 775−782.

(37) Spackman, M. A. *J. Phys. Chem.* **1987**, *91*, 3179−3186.

(38) Brown, A. S.; Spackman, M. A. *Mol. Phys.* **1994**, *83*, 551−566.

(39) Huber, H. *J. Chem. Phys.* **1985**, *83*, 4591−4598.

(40) Hunt, M. J.; Mackay, A. L. *J. Magn. Reson.* **1974**, *15*, 402−414.